Experimental demonstration of generating arbitrary total angular momentum states

Heng Zhou (周 恒)[1,2], Chunqing Gao (高春清)[1,2], Shiyao Fu (付时尧)[1,2,*], Yanwang Zhai (翟焱望)[1,2], and Jianqiang Zhang (张建强)[1,2]

[1]*School of Optics and Photonics, Beijing Institute of Technology, Beijing 100081, China*
[2]*Key Laboratory of Photoelectronic Imaging Technology and System, Ministry of Education, Beijing 100081, China*
**Corresponding author: fushiyao@bit.edu.cn*

Received May 21, 2020; accepted July 14, 2020; posted online September 15, 2020

We experimentally demonstrated an approach to generate arbitrary total angular momentum (TAM) states by using two liquid crystal devices. Photons' TAM, the sum of spin and orbital angular momenta (SAM and OAM) under paraxial approximation, has found many applications in optics and attracted increasing attention in recent years. Our approach is based on the orthogonality of two eigen SAM components, that arbitrary TAM states will be produced through encoding different holograms in one system. The comparison with theoretical predications yields an excellent agreement, including both the separable state and the non-separable state. The proposed scheme takes a step forward for generating complex structured fields and broadens its application to various fields like laser processing and large capacity data transmission.

Keywords: diffraction gratings; polarization.
doi: 10.3788/COL202018.110503.

The concept of photons' angular momentum was originally proposed by Poynting in 1909[1], which is known as spin angular momentum (SAM)[2]. SAM has two eigen values $\sigma = \pm 1$, corresponding to the right and left circular polarizations of a beam, and the SAM value of each photon is $S = \sigma\hbar$, with $\hbar$ the Planck constant divided by 2π. There is another kind of angular momentum for photons simultaneously, known as the orbital angular momentum (OAM), which associates with the spatial wavefront and is independent of polarizations[3,4]. In 1992, Allen *et al.* first pointed out that the Laguerre–Gaussian mode with a helical phase $\exp(il\phi)$ carrying the OAM, where l is an integer called the topological charge and ϕ is the azimuthal angle[5]. The OAM value of each photon in such a mode is $L = l\hbar$. The total angular momentum (TAM) is the sum of the SAM and the OAM under the paraxial approximation, which represents the angular momentum of each photon with $J = (\sigma + l)\hbar$, and thus describes the more complex modes or optical fields.

For a beam carrying the TAM, one can divide it into two categories according to whether it can be separated or not[6]. The separable state can be written as a single direct product of the spin state and the orbital state. Otherwise, a beam is a non-separable state. Separable states have a homogeneous polarization distribution across their wavefront such that the spin and orbital states can be determined separately, while the non-separable states usually have an isotropic polarization. A scalar vortex beam is a kind of separable TAM state, whereas non-separable states have been found in vector vortex beams[7], Poincaré beams[8], etc. Both scalar vortex beams and complex structured OAM-carrying beams are widely used and have various applications in optical communication[9], rotation detection[10], optical tweezers[11], quantum entanglement[12], etc.

There are many methods used to generate TAM states, such as a Sagnac interferometer[13], a Twymann–Green interferometer[14], a Wollaston prism[15], and other methods[16–19]. However, all those methods focus on the TAM states on one single Poincaré sphere. In other words, it is unable to produce more complex TAM states on cascaded Poincaré spheres. Nowadays, a Q-plate (liquid crystals device)[20], an S-plate (sub-wavelength device)[21], and a J-plate (metasurface device)[22] have already been employed to accomplish spin to orbital conversion. Based on their work, Huang *et al.* generated versatile TAM states using cascaded J-plates and realized independent phase control of two arbitrary orthogonal polarizations[6]. This device could generate four possible TAM states by cascading two J-plates, and as the number of cascaded waves increases, the number of the generated TAM states increases. Nevertheless, these schemes still have restrictions inherent in their construction: the output TAM states are constrained to fixed values (e.g., two J-plates can generate up to four various TAM states). Besides, for cascaded J-plate system, the more TAM states generated, the more J-plates are employed and the more complex the system is.

Liquid crystals (LCs) are a state of matter that has properties between those of conventional liquids and solid crystals. Due to its flexible characteristic of modulation, there are many applications in optics such as a liquid crystal spatial light modulator (LC-SLM). The most versatile phase-only LC-SLMs can reconfigure the phase retardation of a beam transmitted through or reflected from each pixel without changing its intensity. LC-SLMs have

widespread applications ranging from three-dimensional projection[23], quantum[24], to adaptive optics[25] and additive manufacturing[26].

In this Letter, we demonstrate a system consisting of two cascaded LC-SLMs to generate arbitrary TAM states. In the proposed system, such two LC-SLMs determine multiple OAM states of two eigen SAM components[27,28]. Based on Lin's method[29] and pattern search iteration algorithm[30], various holograms are computed and can implement any complex OAM states and any phase difference. Any TAM states can be performed through encoding different holograms without replacing any elements in the system. We conduct theoretical derivations, and the proof-of-concept experiment results fit well with theory, which shows the feasibility of this system.

A Jones matrix is employed first to describe the mathematics behind the system. Here we use a pair of orthogonal circular polarization bases $|L\rangle = (1, i)^T/\sqrt{2}$ (left circular polarization, LCP), $|R\rangle = (1, -i)^T/\sqrt{2}$ (right circular polarization, RCP) for analysis. We write the azimuthal phase $\exp(il\phi)$ as $|l\rangle$ for brevity and highlight that the derivation is under a paraxial approximation. For horizontally linear polarization, the incident light field Ψ_{in} can be expressed as

$$|\Psi_{\text{in}}\rangle = |L\rangle|0\rangle + |R\rangle|0\rangle. \tag{1}$$

Arbitrary TAM states, including both separable and non-separable states, universally read as

$$|\Psi_{\text{out}}\rangle = |L\rangle \sum \eta|l_L\rangle + |R\rangle \sum \xi|l_R\rangle, \tag{2}$$

where $|l_L\rangle$ and $|l_R\rangle$ correspond to the OAM states of LCP and RCP; η and ξ are the complex amplitudes of different $|l_L\rangle$ and $|l_R\rangle$, respectively. For generating arbitrary TAM states, we need to separately modulate the left and right circular polarization components. As for LC-SLMs, only a specific polarization can be phase-only modulated[31] while the corresponding orthogonal component is unaffected. Due to LC-SLM's polarization-sensitive properties, here we use two LC-SLMs to modulate LCP and RCP components separately and use $|\text{SLM1}\rangle$ and $|\text{SLM2}\rangle$ to briefly describe the phase modulation. Such generation requires some polarization devices like a half-wave plate (HWP) and a quarter-wave plate (QWP), whose Jones matrices are

$$M_{\frac{\lambda}{2}}(\theta) = \begin{pmatrix} \cos 2\theta & \sin 2\theta \\ \sin 2\theta & -\cos 2\theta \end{pmatrix} \tag{3}$$

and

$$M_{\frac{\lambda}{4}}(\theta) = \begin{pmatrix} \cos^2\theta + i\sin^2\theta & \sin\theta\cos\theta(1-i) \\ \sin\theta\cos\theta(1-i) & \sin^2\theta + i\cos^2\theta \end{pmatrix}, \tag{4}$$

where θ is the angle of the fast axis of the HWP or QWP. As sketched in Fig. 1, by using two HWPs, one QWP, and two SLMs, the conversion can be expressed as

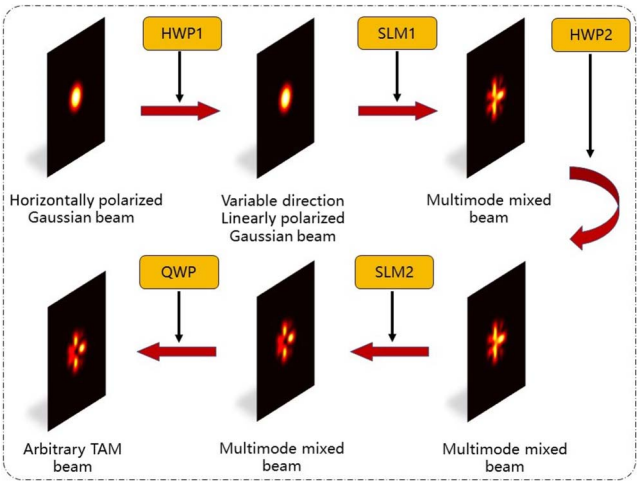

Fig. 1. Principle of generating arbitrary TAM states.

$$\begin{aligned} |\Psi_{\text{out}}\rangle &= M_{\frac{\lambda}{4}}(45°)|\text{SLM2}\rangle^{-1} M_{\frac{\lambda}{2}}(45°)|\text{SLM1}\rangle M_{\frac{\lambda}{2}}(\theta)|\Psi_{\text{in}}\rangle \\ &= e^{i(-45°)} \cos 2\theta |L\rangle|\text{SLM1}\rangle \\ &\quad + e^{i(45°)} \sin 2\theta |R\rangle|\text{SLM2}\rangle^{-1}. \end{aligned} \tag{5}$$

Here, $|\text{SLM2}\rangle^{-1}$ represents that SLM2 not only modulates the incident beam, but also changes the chirality through reflection. Compared with Eq. (2), we can find that the amplitude and phase of the complex amplitudes η and ξ are determined by θ (the rotation angle of HWP1) and SLMs, respectively. The OAM states $|l_L\rangle$ and $|l_R\rangle$ are determined by SLMs. By changing the rotation angle θ and the holograms on SLMs, we can get arbitrary TAM outputs.

To generate arbitrary TAM states following the above procedures, various specially-designed holograms must be encoded on two SLMs separately to generate controllable multiplexed scalar vortex beams. This kind of light field regulation needs both amplitude and phase modulation. However, the SLM we used here is a phase-only device, and phase modulation individually causes partial loss of the incident beam[27]. Also, it is impossible to simultaneously import amplitude modulation and phase modulation into one pixel. Therefore, the energy ratio between different modes cannot fully satisfy the design requirements.

To accomplish the desired OAM proportion through a single phase-only grating, iterations must be introduced. Here Lin's method[29] and pattern search iteration algorithm[30] are employed. In the calculation by continuously collecting and analyzing the practical OAM spectra of the far-field construction from the holograms, the parameters of the holograms are appropriately changed according to the difference between the practically obtained mode and the desired mode, thus to make the optical fields generated from the hologram infinitely close to the desired fields. We design three multimode mixed holograms whose OAM state distributions are $(|-1\rangle + |+2\rangle)$, $(|-4\rangle + |-3\rangle + |+1\rangle)$ and $(|-4\rangle + |-3\rangle + |+1\rangle)e^{i\pi}$, respectively. Such holograms and their corresponding far-field diffraction patterns and OAM spectra are given in Fig. 2.

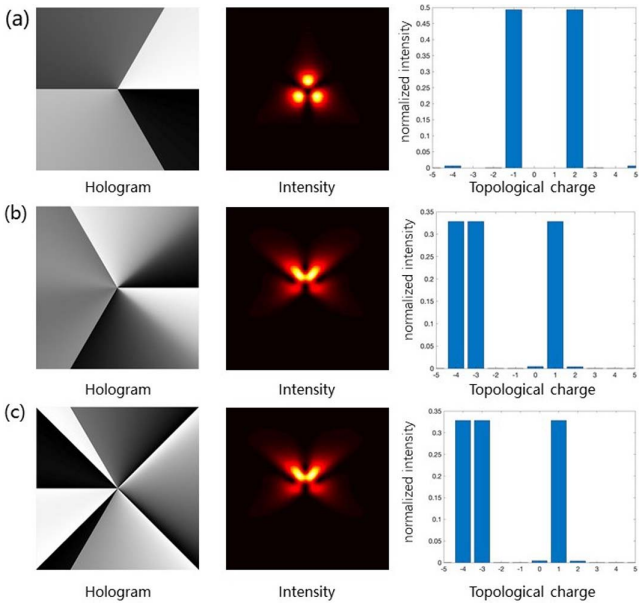

Fig. 2. Holograms to generate multiplexed scalar vortex beams, and their corresponding far-field diffraction patterns and OAM spectra. The OAM state distributions are (a) $(|-1\rangle+|+2\rangle)$, (b) $(|-4\rangle+|-3\rangle+|+1\rangle)$, and (c) $(|-4\rangle+|-3\rangle+|+1\rangle)e^{i\pi}$.

Figure 3(a) shows the experimental setup of generating arbitrary TAM states. A fundamental Gaussian beam with a wavelength of 1.6 μm is incident into a polarized beam splitter (PBS), and then transformed into horizontal polarization. The PBS can be replaced by a horizontally placed polarizer. A half-wave plate (HWP) can modulate the direction of linear polarization. Here, a rotatable HWP (HWP1) is placed behind the PBS and is employed to determine the direction of linear polarization, thus to adjust the final output amplitude ratio of the two SAM components (LCP and RCP). Next comes two LC-SLMs (Holoeye, PLUTO-TELCO-013-C). The hologram on SLM1 controls the OAM spectral distribution and the phase of the horizontal polarization component (the final output beam's LCP portion). Another HWP, the HWP2 whose fast axis is 45° arranged, is placed between SLM1 and SLM2 to exchange the horizontal and vertical polarizations with each other. SLM2 is encoded by another hologram to determine the OAM spectra and the phase of the vertical polarization component (the final output beam's RCP portion). The fast axis of QWP1 is fixed at 45° to transform the orthogonal linear polarization bases into orthogonal circular polarization bases. Finally, the TAM states are produced.

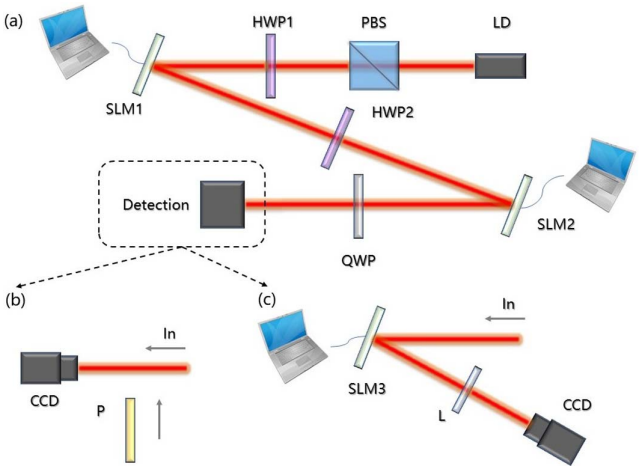

Fig. 3. The experimental setups for generating and testing arbitrary TAM states. LD, laser diode; PBS, polarized beam splitter; HWP1 & 2, half-wave plate; SLM1–SLM3, liquid-crystal spatial light modulator; QWP, quarter wave plate; P, polarizer; L, convex lens; CCD, infrared CCD camera. (a) Generating arbitrary TAM states. (b) Detection of vector polarization properties. (c) Detection of OAM distributions.

Next, we will discuss how to determine the parameters in Eq. (2) through the proposed setup. Eq. (2) can also be written as

$$|\Psi_{\text{out}}\rangle = |\eta_{\text{NOR}}|\left(|L\rangle\sum\eta'|l_L\rangle + \frac{|\xi_{\text{NOR}}|}{|\eta_{\text{NOR}}|}|R\rangle\sum\xi'|l_R\rangle\right), \tag{6}$$

where η' and ξ' are the normalized complex amplitudes. $|\eta_{\text{NOR}}|$ and $|\xi_{\text{NOR}}|$ are the normalization coefficients of the complex-valued columns $\{\eta_n\}$ and $\{\xi_{\text{m}}\}$. One can find easily from Eq. (6) that the generated TAM states are associated with both the multiplexed OAM states and amplitude proportion of the orthogonal circular polarization bases. In the cascaded two-SLM setup, the multiplexed OAM states ($\Sigma\eta'|l_L\rangle$ and $\Sigma\xi'|l_R\rangle$) can be determined directly through the holograms encoded on SLM1 and SLM2 separately, and the intensity proportion $|\xi_{\text{NOR}}|/|\eta_{\text{NOR}}|$ is controlled by rotating HWP1.

To investigate the generation performance of the proposed scheme, two different TAM detection setups are also built. Figure 3(b) shows the detection part of the detecting vector polarization properties. An infrared CCD camera (Xenics, Bobcat-320-star) is used to observe the light field either with a polarizer (P) in the path (placed in the directions of horizontal, 45°, and vertical) or not. Figure 3(c) shows the detection part of the OAM state distributions, where SLM3 encodes a 3×3 Damman vortex grating[32–35]. The CCD camera is placed in the imaging plane of the lens (L) to capture the far-field diffraction patterns.

To examine the reliability of the system we focus on two cases, the separable state and non-separable state. For the separable state, at an instance the holograms that can produce the single OAM mode with $l=+1$ and $l=+3$ are selected and encoded on SLM1 and SLM2, respectively. According to Eq. (5), by rotating HWP1, the output beam should be $|L\rangle|+1\rangle$ when the rotation angle $\theta=0°$ and $|R\rangle|+3\rangle$ when $\theta=45°$. Figure 4 shows the distribution of these two states. They both have single-ring annuli intensity profiles. The polarization state of the beam is a

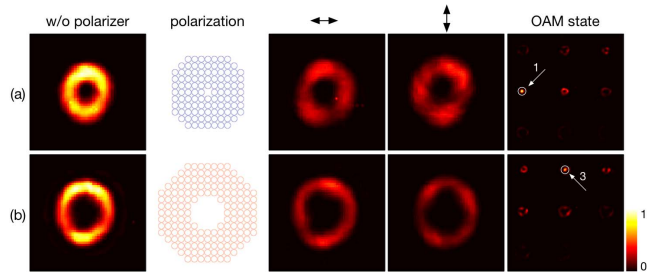

Fig. 4. Experimental results of generating separable TAM states. (a) $|L\rangle|+1\rangle$ and (b) $|R\rangle|+3\rangle$.

uniform circular polarization. Through a Damman grating, the far-field diffraction patterns of the incident beam where the bright spots are present at the desired positions can be observed in the detection part through the setup in Fig. 3(c).

Then we consider the second case, non-separable states. According to the OAM spectra of two eigen SAM components, the non-separable states can be divided into two conditions. One is expected to have homogeneous transverse polarizations. Such states can be represented by one or multiple cascaded Poincaré spheres[6], where the north and south poles have identical OAM spectra. The other has anisotropic transverse polarizations that result from the different OAM spectra of the two eigen SAM components. Such states are also known as vector vortex beams or Poincaré beams[7,8,36].

Figure 5 gives the experimental results of generating one of non-separable TAM states with homogeneous transverse polarizations. In this case, the rotation angle of HWP1 in Fig. 3 is fixed to 22.5° to obtain linear polarizations. First, SLM1 and SLM2 encode the same hologram that can produce coaxial multiplexed OAM to generate non-separable TAM states $|\Psi\rangle = |R\rangle(|-3\rangle+|-1\rangle+|+1\rangle+|+3\rangle)+|L\rangle(|-3\rangle+|-1\rangle+|+1\rangle+|+3\rangle)$. Because of the identical amplitudes between LCP and RCP, the output beam is horizontally linear polarized. It is evidenced by the distribution of the light field after passing through the horizontally and vertically placed polarizers [through the setup in Fig. 3(b)], as shown in Fig. 5(a).

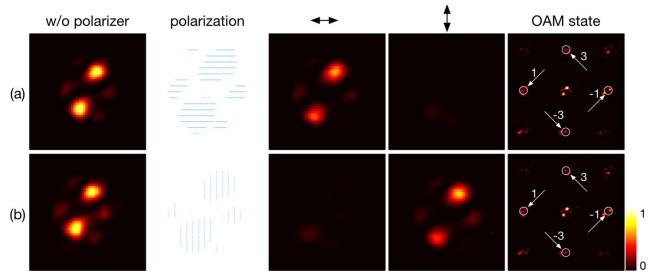

Fig. 5. Experimental results of generating non-separable TAM states with homogeneous transverse polarizations. (a) $|\Psi\rangle = |R\rangle(|-3\rangle+|-1\rangle+|+1\rangle+|+3\rangle)+|L\rangle(|-3\rangle+|-1\rangle+|+1\rangle+|+3\rangle)$, and (b) $|\Psi\rangle = |R\rangle(|-3\rangle+|-1\rangle+|+1\rangle+|+3\rangle)+\exp(i\pi)|L\rangle(|-3\rangle+|-1\rangle+|+1\rangle+|+3\rangle)$.

After passing through a 3×3 Damman grating encoded on SLM3, bright spots appear at the center of four diffraction orders, -3, -1, $+1$, and $+3$, indicating that the OAM state distribution meets our desires. When we change the phase difference of LCP and RCP into π through replacing the hologram on SLM2, the output beam is $|\Psi\rangle = |R\rangle(|-3\rangle+|-1\rangle+|+1\rangle+|+3\rangle)+\exp(i\pi)|L\rangle(|-3\rangle+|-1\rangle+|+1\rangle+|+3\rangle)$, as shown in Fig. 5(b). Compared with the state in Fig. 5(a), it turns out to be vertically linear polarizations, but with both intensity distribution and OAM states unchanged. Actually, two generated TAM states in Fig. 5 are located at two various points on the equator of the same group of cascaded Poincaré spheres.

Figure 6 presents the experimental results of generating non-separable TAM states with anisotropic polarizations, namely, the complex vector vortex states ($|\Psi\rangle = |R\rangle(|-1\rangle+|+1\rangle)+|L\rangle|+2\rangle$). Such TAM states can be acquired if we encode different holograms on SLM1 and SLM2, where SLM1 is to generate a scalar vortex $|+2\rangle$ and SLM2 is to generate a two-fold multiplexed scalar vortex $(|-1\rangle+|+1\rangle)$. Meanwhile, the fast axis of HWP1 is 22.5° arranged. In this case, photons in the two SAM components have different OAM state distributions, and thus the polarization state of the beam should exhibit an anisotropic distribution. The characterization of the anisotropic distribution is that the beam intensity can be observed in all polarization states. Results of this measurement are also given in Fig. 6. We collect the beam intensity in three typical polarization directions 0° (horizontal), 45°, and 90° (vertical). The intensity distribution can be observed in all three directions. For the OAM detection, we rotate HWP1 to make sure that LCP and RCP emit separately. Through the Damman grating, bright spots appear at the center of the ±1 diffraction order for RCP and the $+2$ diffraction order for LCP. Both the intensity distribution and OAM states are consistent with the desired.

In summary, we have demonstrated a scheme of generating arbitrary TAM states through cascading two SLMs. In the proof-of-concept experiment, both the separable states and non-separable states are generated. All these three examples fit well with the expectations.

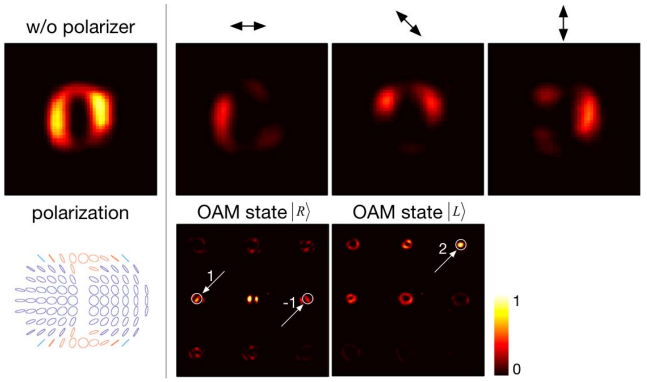

Fig. 6. Experimental results of generating non-separable TAM states with anisotropic transverse polarizations. The generated TAM state is $|\Psi\rangle = |R\rangle(|-1\rangle+|+1\rangle)+|L\rangle|+2\rangle$.

Although the implemented cases are relatively simply designed, the design principles can be applied to any combination of SAM and OAM using different holograms. That means the proposed single system can generate arbitrary TAM states without replacing any elements. What we should do is to change the two holograms on the two SLMs, meanwhile adjusting the fast axis orientation of HWP1. The proposed scheme paves the way for generating complex structured fields, and the flexible phase programmable idea will inspire tunable device generation and beam shaping, with diverse applications in laser processing, remote sensing, and so on.

This work was supported by the National Natural Science Foundation of China (NSFC) (Nos. 11834001 and 61905012), the National Postdoctoral Program for Innovative Talents of China (No. BX20190036), the China Postdoctoral Science Foundation (No. 2019M650015), and the Beijing Institute of Technology Research Fund Program for Young Scholars.

References

1. J. H. Poynting, Proc. R. Soc. Lond. A **82**, 560 (1909).
2. R. A. Beth, Phys. Rev. **50**, 115 (1936).
3. Y. Shen, X. Wang, Z. Xie, C. Min, X. Fu, Q. Liu, M. Gong, and X. Yuan, Light Sci. Appl. **8**, 90 (2019).
4. A. M. Yao and M. J. Padgett, Adv. Opt. Photon. **3**, 161 (2011).
5. L. Allen, M. W. Beijersbergen, R. J. C. Spreeuw, and J. P. Woerdman, Phys. Rev. A **45**, 8185 (1992).
6. Y. Huang, N. A. Rubin, A. Ambrosio, Z. Shi, R. C. Devlin, C. Qiu, and F. Capasso, Opt. Express **27**, 7469 (2019).
7. Q. Zhan, Adv. Opt. Photon. **1**, 1 (2009).
8. S. Fu, Y. Zhai, T. Wang, Y. Ci, and C. Gao, Appl. Phys. Lett. **111**, 211101 (2017).
9. T. Lei, M. Zhang, Y. Li, P. Jia, G. N. Liu, X. Xu, Z. Li, C. Min, J. Lin, C. Yu, H. Niu, and X. Yuan, Light Sci. Appl. **4**, e257 (2015).
10. M. P. J. Lavery, F. C. Speirits, S. M. Barnett, and M. J. Padgett, Science **341**, 537 (2013).
11. M. J. Padgett and R. Bowman, Nat. Photonics **5**, 343 (2011).
12. R. Fickler, R. Lapkiewicz, W. N. Plick, M. Krenn, C. Schaeff, S. Ramelow, and A. Zeilinger, Science **338**, 640 (2012).
13. P. H. Jones, M. Rashid, M. Makita, and O. M. Maragò, Opt. Lett. **34**, 2560 (2009).
14. S. Fu, C. Gao, Y. Shi, K. Dai, L. Zhong, and S. Zhang, Opt. Lett. **40**, 1775 (2015).
15. J. Xin, C. Gao, C. Li, and Z. Wang, Appl. Opt. **51**, 7094 (2012).
16. B. Khajavi and E. J. Galvez, J. Opt. **18**, 084003 (2016).
17. H. Zhang, L. Yao, Y. Pang, and J. Xia, Chin. Opt. Lett. **16**, 092601 (2018).
18. W. Zhang and L. Chen, Chin. Opt. Lett. **16**, 030501 (2018).
19. J. H. Clegg and A. A. Neil, Opt. Lett. **38**, 1043 (2013).
20. L. Marrucci, C. Manzo, and D. Paparo, Phys. Rev. Lett. **96**, 163905 (2006).
21. M. Gecevicius, M. Ivanov, M. Beresna, A. Matijosius, V. Tamuliene, T. Gertus, A. Cerkauskaite, K. Redeckas, M. Vengris, V. Smilgevicius, and P. G. Kazansky, J. Opt. Soc. Am. B **35**, 190 (2018).
22. R. C. Devlin, A. Ambrosio, N. A. Rubin, J. P. B. Mueller, and F. Capasso, Science **358**, 896 (2017).
23. H. Sasaki, K. Yamamoto, K. Wakunami, Y. Ichihashi, R. Oi, and T. Senoh, Sci. Rep. **4**, 6177 (2014).
24. K. H. Kagalwala, G. Di Giuseppe, A. F. Abouraddy, and B. E. A. Saleh, Nat. Commun. **8**, 739 (2017).
25. N. Ji, Nat. Methods **14**, 374 (2017).
26. M. Shusteff, A. E. M. Browar, B. E. Kelly, J. Henriksson, T. H. Weisgraber, R. M. Panas, N. X. Fang, and C. M. Spadaccini, Sci. Adv. **3**, eaao5496 (2017).
27. A. Forbes, C. Rosales-Guzmán, and N. Bhebhe, Opt. Express **25**, 25697 (2017).
28. Fuentes, J. L. Martínez, and I. Moreno, Opt. Express **26**, 5875 (2018).
29. J. Lin, X. C. Yuan, S. H. Tao, and R. E. Burge, Opt. Lett. **30**, 3266 (2005).
30. L. Zhu and J. Wang, Opt. Express **23**, 26221 (2015).
31. I. Moreno, J. A. Davis, T. M. Hernandez, D. M. Cottrell, and D. Sand, Opt. Express **20**, 364 (2012).
32. N. Zhang, X. C. Yuan, and R. E. Burge, Opt. Lett. **35**, 3495 (2010).
33. S. Fu, S. Zhang, T. Wang, and C. Gao, Opt. Express **24**, 6240 (2016).
34. N. Zhang, J. A. Davis, I. Moreno, D. M. Cottrell, and X. C. Yuan, Opt. Express **18**, 25987 (2010).
35. I. Moreno, J. A. Davis, K. Badham, M. M. Sánchez-López, J. E. Holland, and D. M. Cottrell, Sci. Rep. **7**, 2216 (2017).
36. E. J. Galvez, in *Photonics: Scientific Foundations, Technology and Applications* 1, David L. Andrews, Ed. (Wiley, 2015), p. 61.